Free vibration behaviour of thin-walled concrete box-girder bridge using Perspex sheet experimental model

V. Verma [a,*], K. Nallasivam [b]

[a] Research Scholar, Department of Civil Engineering, National Institute of Technology, Hamirpur-177005, India

[b] Assistant Professor, Department of Civil Engineering, National Institute of Technology, Hamirpur-177005, India

* Corresponding e-mail address: virajan75409@gmail.com

ORCID identifier: https://orcid.org/0000-0002-4673-8209 (V.V.)

ABSTRACT

Purpose: Curved box-girder bridges offers an excellent solution to the problems associated with traffic congestion. However, owing to their complex geometry, they are subjected to shear lag, torsional warping and cross-sectional distortion, which must be assessed in their study and design. Furthermore, the dynamic behaviour of curved bridges adds to the complexity of the issue, emphasizing the importance of studying free vibration. The purpose of this study is to numerically model the concrete curved box-girder bridge considering torsional warping, distortion and distortional warping effects and to identify key parameters that influence the free vibration response of the box-girder bridge by validating it with experimental and analytical studies.

Design/methodology/approach: The concrete bridge is numerically modelled by means of computationally effective thin-walled box-beam finite elements that consider torsional warping, distortion and distortional warping, which are prominent features of thin-walled box-girders. The free vibration analysis of the concrete curved box-girder bridge is performed by developing a finite element based MATLAB program.

Findings: The identification of critical parameters that influence the free vibration behaviour of curved thin-walled concrete box-girder bridges is one of the main findings of the study. Each parameter and its effect has been extensively discussed.

Research limitations/implications: The study limits for the preliminary design phase of thin-walled box-girder bridge decks, where a complete three-dimensional finite element analysis is unnecessary. The current approach can be extended to future research using a different method, such as finite element grilling technique on multi-span curved bridges having unequal span.

Originality/value: The current research implements a finite element formulation in combination with thin-walled beam theory, where an extensive parametric study is conducted on the free vibration behaviour of a concrete thin-walled box-girder bridge, while also accounting for their complex structural actions. The validity of the given numerical formulation is demonstrated by a comparison of the natural frequencies found experimentally. The study carried out will be of great importance for engineers to help them anticipate the modal characteristics of a curved concrete thin-walled girder bridge, which will further be useful for evaluating their dynamic response analysis.

ANALYSIS AND MODELLING

1. Introduction

Bridges with curved alignments were once uncommon. Nonetheless, technology has advanced, and new bridges and traffic separation systems are frequently constructed on a horizontal curve. Increased traffic volumes and speeds, geometric limitations of the urban landscape, and enhanced structural forms that conform themselves to curved construction have all contributed to this. One such structural type is the concrete box girder that can span long distances. The cross section of such frameworks is intrinsically high in torsion. This property becomes vital, since curvature causes strong torsion stresses. Concrete is also suitable for curved construction since it can be easily shaped into the desired form. As a result of these factors, concrete box girders have become the preferred structure form in several jurisdictions.

A bridge is a structure constructed over a road, river or railway for people and vehicles to move through. The Roman Empire built a 6-metre-wide wooden bridge at the end of the 2nd century AD, marking the first ever use of bridges. However, the use of curved bridges has become much more prominent in recent years and as a result, box beam elements with unparalleled torsional and bending rigidities are used [1]. The advantages of curved bridges include: attractive and economical structural designs, higher stiffness-to-mass ratios, greater stability and serviceability, thinner sections, fewer traffic congestion and ideally suited for complex interchanges that could have geometric constraints such as river crossings. That being said, the inherent structural complexities, including torsional warping and distortion effects, present major difficulties in its structural design [2].The solution to this problem lies in the availability of digital computers that can handle complex mathematical computations with ease [3].

Modal analysis has gained worldwide recognition in recent decades for a variety of applications, Ewins, (2000) [4]. Bridges and buildings are perhaps the most commonly encountered structures with this application in the context of civil engineering. The extraction of modal parameters (frequencies, damping ratios, and mode shapes) from measurements of dynamic responses is referred to as experimental modal analysis. These modal parameters are used to update finite element models, Friswell and Mottershead (1995) [5], identify structural damage Ren and De Roeck (2002) [6], and evaluate structural safety Ren et al. (2004) [7]. Current modal identification techniques, on the other hand, are restricted to regulated laboratory experiments in which a low level excitation is provided and the resulting system response is recorded. Actual operating environments are likely to vary greatly from those used in laboratory modal research. As a result, it is often necessary to define modal prototypes of actual civil engineering systems under operating conditions.

In general, the experimental modal analysis technique is carried out using frequency response functions (FRFs) in the frequency domain or impulse response functions (IRFs) in the time domain, based on both input and output measurement data. The direct records of the sensors that are located at multiple locations are the dynamic responses (output) for civil engineering structures. That being said, it is clear that excitation of the actual structure in its operating state is difficult and expensive. It is exceedingly difficult to quantify the input excitation forces acting on a massive structure. While forced vibrations (like heavy shakers and drop weights) and synchronized input–output measurements are often possible, these methods are limited in real-world applications due to testing, structural complexity, and data quality.

Dynamic loading is the principal cause of bridge vibration. Due to the curvature effect, the dynamic response of the curved bridges is much more complex and less understood than the straight bridges. The dynamic resistance of box-girder bridges is much higher than classical bridges. Box-girder bridges operate effectively for railroad structures as well as for highways, with the former having greater ability to carry live loads. Dynamic loads are indeed a key component for all bridges and therefore understanding their response to these loads is of paramount importance. The study of free vibration forms the basis for the dynamic response of a bridge and for checking whether the bridge is

safe under the vibration induced by the dynamic load. The free vibration features of any structure including modal parameters such as mode shapes and natural frequencies have to be studied in order to truly comprehend its fundamental dynamic behaviour [8]. Every system tends to vibrate during certain frequencies, which are called natural frequencies. The system appears to assume a certain shape when it vibrates under that natural frequency without any external force, which is called the mode shape. Modes are a function of the material properties of that system, such as stiffness, mass and damping. The total number of modes to be considered for a complete investigation of the frequency excitation is determined by the Effective mass participation factor. A mode having a greater effective mass is likely to be a major contributor to the system's response and is easily simulated by base excitation. On the other hand, this means that modes with small effective masses can-not be easily excited. The total number of modes used should be sufficient to ensure that at least 90% of the actual mass is taken as the total effective modal mass of the model. The effective mass participation factor, p_i is represented as:

$$p_i = \frac{\Phi_i[M]r}{(\Phi_i[M]\Phi_i)^2}$$ Eq. (1)

where, Φ_i represents normalized mode shapes, $[M]$ is the mass matrix and r is the ground motion influence coefficient.

Substantial research has been reported in the past on the behaviour of box-girder bridges. With the contribution of thin-walled beam theory, Vlasov, (1961) in [9] is regarded to be the leading proponent in the field of box-girder bridges. Maisel, (1985) in [10] amended Vlasov's general coordinate method to counteract torsional and distortional effects in thin-walled beams. Boswell and Li, (1995) in [11] examined the relationships between torsional stress and distortion warping for the analyses of thin-walled beams. Jönsson, (1999) in [12] presented a structured framework for the distortion of thin-walled beams by developing a general differential equation. Zhang et al., (2010) in [13] investigated the effect of shear lag in thin-walled box-girder bridges through experimental and numerical analysis. Awall et al. 2012 [14] explored the impact of bottom bracing on the torsional dynamic properties of curved twin I-girder bridges. Experimental and computational simulations were conducted by [15] for the static response of thin-walled box girder bridges. The static and vibrational properties of curved thin-walled box beams were investigated by Kashefi et al., in [16] through various experiments. Tsiptsis and Sapountzakis, (2018) in [17] carried out an isogeometric analysis on the

dynamic behavior of curved structures, taking into account the warping effects. Tsiptsis and Sapountzakis, (2017) in [18] formulated advanced stiffness matrices for the dynamic analysis of curved bridges by taking into account distinct warping parameters. Sapountzakis and Tsiptsis, (2017) in [19] used Finite Element Method based Isogeometric methods to analyse the vibrations of thin or thick walled homogeneous beams, which included warping and shear deformation effects. Tsiptsis and Sapountzakis, (2017) in [20] used isogeometric techniques to assess curved beams with thin or thick-walled cross sections, taking nonuniform warping, shear deformation, and distortion effects into account.

Thin-walled box bridge study involves a variety of methods, such as finite difference and finite stripes. Cheung and Cheung, (1971) in [21] was the first to apply finite strip technique for the investigation of slab bridges. Heins and Oleinik, (1976) in [1] implemented the finite difference technique by considering torsional and cross-sectional distortions in curved box-beam bridges. A pre-stressed concrete box-girder bridge was assessed by Abdullah and Abdul-Razzak, (1990) in [22] using finite strip technique and incorporating bending and in-plane strips of higher order. Kermani and Waldron, (1993) in [2] successfully applied the stiffness theory to examine straight box-girders which included warping torsion and distortion.

Various concepts and research techniques have been proposed for the evaluation of box-girder bridges, but the approach to finite element analysis is widely considered as being the most robust. Fam and Turkstra, (1975) in [23] proposed a finite element box-bridge model with different combinations of straight and horizontal curved segments. Gunnlaugsson and Pedersen, (1982) in [24] introduced a finite element model for thin-walled beams, considering seven degrees of freedom on each node. The distortion problem in thin-walled box spine beams was resolved by Boswell, S.H. Zhang, (1984) in [25] using finite element methodology. Hsu et al., (1990) in [26] introduced a more realistic finite element beam model and developed the stiffness matrix using variation approach. Razaqpur and Li, (1994) in [27] put into place Vlasov's thin-walled beam theory coupled with a shear lag warping function to develop a box beam finite element for a thin-walled box-girder bridge. Yaping et al., (2002) in [28] recommended to use a finite curved beam element to evaluate the curved thin-walled box-beam bridge. The behaviour of steel box girder bridges was examined by Begum, (2010) in [29], by using commercially available FEM software ANSYS. Tsiptsis and Sapountzaki, (2020) in [30] proposed a model

in ABAQUS for the static and dynamic analysis of straight and curved composite beams taking into account the friction model.

The finite element methodology was extensively applied by Zhu et al., (2016) in [31] for the vibrational study of thin walled rectangular beams. The flexural response of curved box-girder bridges was measured by Gupta and Kumar, (2018) in [32] using FEM software CSiBridge [33]. Hamza et al. (2019) in [34] presented a non-linear finite element model to estimate ultimate load capacity of horizontally curved steel beams.

Also, different methods have been used by the past researchers to conduct the free vibration analysis of beams and bridges. Mukhopadhyay and Sheikh, (1995) in [3] made use of the finite element method to calculate large amplitude vibration of horizontally curved beams using an isoperimetric three-noded beam element. Noor et al., (1989) in [35] applied some simple finite element models to study the free vibrations of curved thin-walled beams using thin-walled beam theory given by Vlasov, (1961) in [5]. Panicker et al., (2014) in [36] made use of the finite element software ABAQUS for the free vibration analysis of FRP bridges. Yoon et al., (2005) in [37] also conducted the finite element analysis for the free vibration of steel I-girder bridges. Snyder and Wilson, (1992) in [38] applied the closed form solution to calculate the free vibration frequencies of horizontally curved beams. Tabba and Turkstra, (1977) in [39] provided a general solution for the free vibration analysis of thin-walled curved girders using several parameters on natural frequencies. Memory et al. (1995) in [40] applied Rayleigh's method for free vibration analysis of bridges. Kou et al. (1992) in [41] formulated a dynamic theory for the free vibration analysis of curved thin-walled girder bridges which also took into account the effects of warping. Tan et al. (2016) in [42] applied an analytical approach based on Euler-Bernoulli and transfer matrix method beam theory for investigating the free vibration characteristics of simply supported bridge. Awall et al., (2016) in [43] utilised three dimensional finite element method and field measured approach for the free vibration analyses of I-girder bridge. Yin et al., (2018) in [44] made use of the finite element software ANSYS for obtaining the modal analysis parameters of a steel box-girder bridge. Wodzinowski et al., (2018) in [45] conducted a sensitivity analysis to inspect the free vibration response of composite I-girder bridges. A finite element methodology was proposed by Verma and Nallasivam in [46] for thin-walled box-girder bridge under Indian railway loading.

The literature reveals that past researchers have made a decent effort to predict the modal characteristics of box-girders using a wide range of techniques. However, these techniques either result in closed-form solutions that are far too complex to be used by the engineers in practice or the analysis was performed using finite-element approach without considering the torsional warping and distortional warping effects of the box-girder bridge. The current study implements such a finite element formulation developed by Zhang and Lyons (1984) in [47] in combination with thin-walled beam theory that not only predicts the free vibration characteristics of the concrete box-girder bridge accurately, but also takes into account its complex structural actions.

Moreover, very few researchers had conducted such a wide range of parametric studies on the free vibration behaviour of box-girder bridge. The present work identifies six key parameters that influence the modal characteristics of concrete thin-walled box-girder bridge.

The objectives of this study are:
1. One dimensional finite element modelling of thin-walled box beam elements for concrete curved box-girder bridges, which would be computationally efficient.
2. Identifying and predicting the fundamental frequency and mode shapes of a concrete curved box-girder bridge with precision.

2. Assumptions and limitations

The basic assumptions related to the theory of linear elastic small displacement have been taken into consideration. The assumptions states that the material is isotropic, homogeneous and linear elastic and the actual deformations are relatively small compared to the dimensions of the structure. Other assumptions and limitations used in this study include the following:
1. Plane section remains plane, but may not remain perpendicular to the axis of the beam in case of bending and thus shear deformations are allowed.
2. The in-plane longitudinal bending motion of a single component plate is investigated employing elementary beam theory, with distortion-induced shear deformations ignored.
3. The analysis is restricted to situations where the cross-section dimensions are relatively small compared to the length of the span and the radius of the curvature.

4. The stiffness of Diaphragms is assumed to be infinite in their own plane, whereas they are considered to be perfectly flexible perpendicular to the plane.
5. The study is limited to the case where the thickness of the wall is small compared to the cross-section dimensions.

3. Finite element formulation of concrete thin-walled box-girder

3.1. Element geometry

A curved concrete thin-walled box beam element is being shown in Figure 1, where the cross-sections are generated by straight lines. The distortion analysis is simplified by assuming that the axis of symmetry of the cross-section is vertical. This assumption becomes redundant for the analysis of torsion and bending.
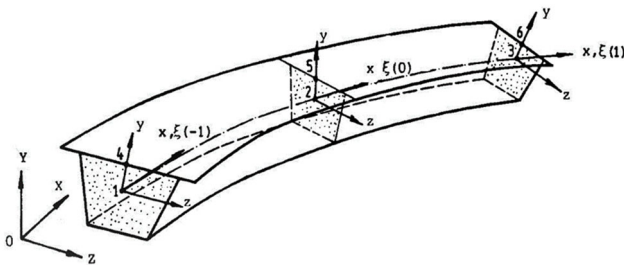

Fig. 1. Three nodded concrete thin-walled box beam element

The element axis is defined as the locus of the centroids which may be eccentric from but parallel to the flexural axis. The elemental nodes positioned on the axis are at the ends and at the mid-point.

A local Cartesian coordinate system (x, y, z) directed towards the axis curve is used to express the element. The origin of the coordinate system is represented by the centroid of the cross-section. It is also presumed that the principal axis of the cross-section matches with the local yz axis direction. The local x axis is directed towards the elemental axis and the tangent from node one to node three. The local y axis denotes the vertical axis of symmetry whereas the local z axis is represented by a right handed orthogonal system.

A natural coordinate ξ is used to express the Global coordinate system, where the value of ξ is taken as -1, 0 and +1 on the three elemental faces. Let $r = X.i + Y.j + Z.k$ denotes the position vector of any point 'P' on the elemental axis, then a unit tangent vector directed towards the x direction is given as

$$e_x = J^{-1}\left(\frac{\partial X}{\partial \xi}i + \frac{\partial Y}{\partial \xi}j + \frac{\partial Z}{\partial \xi}k\right) \qquad \text{Eq. (2)}$$

where i, j and k in the above equation are the unit vectors along global X, Y and Z. The Jacobian factor is given as

$$J = \left[\left(\frac{\partial X}{\partial \xi}\right)^2 + \left(\frac{\partial Y}{\partial \xi}\right)^2 + \left(\frac{\partial Z}{\partial \xi}\right)^2\right]^{1/2} \qquad \text{Eq. (3)}$$

The cross product of e_x and e_y gives the unit tangent vector in the local z direction

$$e_z = e_x \times e_y \qquad \text{Eq. (4)}$$

3.2. Relationship between stress and strain

The displacements can be represented in local and global coordinate system. The following equation gives the displacements in local coordinate system as:

$$\bar{\delta} = \left[u, v, w, \theta_x, \theta_y, \theta_z, \theta_x', \gamma_d, \gamma_d'\right]^T \qquad \text{Eq. (5)}$$

where u, v and w in the above equation represents the translations in local x, y and z axes respectively, θ_x represents twisting angle, θ_x' represents twisting rate, by θ_y and θ_z represents rotation around y and z axes respectively, γ_d represents angle of distortion and γ_d' represents distortion rate. The Poisson's ratio induced effects are important when transverse bending stresses caused by cross-section distortion have same magnitude as the longitudinal stresses caused by longitudinal bending, torsional and distortional warping. In such situations, the Poisson's ratio effects in transverse bending may produce significant longitudinal bending stresses in the box section's individual component plates. The Distortion is due to the combined effect of torsion as well as Poisson's ratio as can be seen in Equation 8.

The displacements can also be represented in global coordinate system as

$$\delta = \left[U, V, W, \varphi_x, \varphi_y, \varphi_z, \theta_x', \gamma_d, \gamma_d'\right] \qquad \text{Eq. (6)}$$

where U, V and W in the above equation represents the translations in global x, y and z axes respectively and φ_x, φ_y and φ_z represents the rotations around the same axes.

There are no changes in twisting rate θ_x', angle of distortion γ_d and distortion rate γ_d' as they remain in local coordinate system. The equations defined above shows that there are nine degrees of freedom per node in the thin-walled box beam element.

The following equation gives the stress vector in its general form as

$$\sigma = \left[N_x, Q_y, Q_z, M_{st}, M_y, M_z, \frac{1}{\mu_t}B_1, M_d, B_{11}\right]^T \qquad \text{Eq. (7)}$$

where N_x in the above equation represents the axial force, Q_y and Q_z represents shear forces, M_{st} represents pure torsional moment, M_y and M_z represents primary bending moments, μ_t represents warping shear parameter, B_1 represents torsional warping bi-moment, M_d represents distortional moment and B_{11} represents distortional warping bi-moment.

The rigidity matrix in its generalized form is

$$D = \begin{bmatrix} EA & & & & & & & & \\ & GA_{sy} & & & & & & 0 & \\ & & GA_{sz} & & & & & & \\ & & & GJ_T & & & & & \\ & & & & EI_y & & & & \\ & & & & & EI_z & & & \\ & & 0 & & & & \frac{1}{\mu_t}E_1J_I & & \\ & & & & & & & E_1J_D & \\ & & & & & & & & E_1J_{II} \end{bmatrix} \qquad \text{Eq. (8)}$$

where E in the above equation represents Young's modulus of Elasticity, G represents shear modulus, A represents the cross-sectional area, A_{sy} and A_{sz} represents effective shear areas along y and z directions respectively, J_T represents torsional moment of inertia, I_y and I_z represents the primary bending moments of inertia around y and z axes respectively, J_I represents the torsional warping moment of inertia, μ_t represents warping shear parameter, J_d represents distortional second moment of area and J_{II} represents the distortional warping moment of inertia. All the parameters of the above equation have been evaluated according to Nallasivam, (2006) in [8]. The conversion modulus of elasticity is defined as below

$$E_1 = \frac{E}{(1-\nu^2)} \qquad \text{Eq. (9)}$$

where ν is the Poisson's ratio.

3.3. Shape functions

The shape functions for axial and flexural effects which requires only C_0 continuity and given as

$$N_i = \frac{1}{2}(\xi^2 + \xi_0) \text{ for } i=1 \text{ and } 3 \qquad \text{Eq. (10)}$$

$$N_i = (1 - \xi_0) \text{ for } i=2 \qquad \text{Eq. (11)}$$

where $\xi_0 = \xi\xi_1$

Since the governing equations for torsion and distortion are fourth order and the beam being three-noded, fifth order C_1 continuity is required for torsion and distortion. The shape functions are given as

$$N_{11} = \left(\frac{\xi^2}{4}\right)(4 - 5\xi - 2\xi^2 + 3\xi^2) \qquad \text{Eq. (12)}$$

$$N_{12} = \left(\frac{J_1}{4}\right)\xi^2(1 - \xi)(1 - \xi^2) \qquad \text{Eq. (13)}$$

$$N_{21} = \left(\frac{\xi^2}{4}\right)(4 + 5\xi - 2\xi^2 + 3\xi^2) \qquad \text{Eq. (14)}$$

$$N_{22} = \left(\frac{J_2}{4}\right)\xi^2(1 + \xi)(\xi^2 - 1) \qquad \text{Eq. (15)}$$

$$N_{31} = (1 - \xi^2)^2 \qquad \text{Eq. (16)}$$

$$N_{32} = J_3\xi(1 - \xi^2)^2 \qquad \text{Eq. (17)}$$

where $\xi_0 = \xi\xi_1$ and J_1, J_2 and J_3 are the Jacobian factors at the three nodes of the element.

The element stiffness matrix may be written as

$$[K^e] = \int_{-1/2}^{1/2}[B]^T[D][B]\,dx = \int_{-1}^{1}J[B]^T[D][B]d\xi \qquad \text{Eq. (18)}$$

The element mass matrix may be written as

$$[M^e] = A\int_{-1/2}^{1/2}[\bar{N}]^T\rho[\bar{N}]\,dx = A\int_{-1}^{1}J[\bar{N}]^T\rho[\bar{N}]d\xi \qquad \text{Eq. (19)}$$

4. Eigen value problem for un-damped system

The general equation of motion for an un-damped free vibration system can be written as

$$[M][\ddot{\delta}] + [K][\delta] = 0 \qquad \text{Eq. (20)}$$

where $[K]$ and $[M]$ are the global stiffness and mass matrix after applying boundary conditions.

Assuming harmonic motion in natural mode of vibration, the response can be written as

$$\{\delta\} = \{X\}sin(\omega t + \varphi) \qquad \text{Eq. (21)}$$

where $\{X\}$ is the vector of nodal amplitude of vibration, ω is the circular natural frequency of vibration [rad/sec] and φ is the phase angle.

Substitution of Eq. (21) in Eq. (20) leads to the generalized eigen value problem.

$$\{[K] - \omega^2[M]\}\{X\} = 0 \qquad \text{Eq. (22)}$$

Eq. (22) is solved using a standard eigen solver to obtain the values of natural frequencies and mode shapes of the box-girder bridge.

5. Experimental and analytical validation

The validation of the current research is done in this section through experimental and analytical studies. The results, which are in close proximity to previous research findings, demonstrate the authenticity and generality of the finite element formulation implemented.

5.1. Experimental validation through Perspex sheet box-girder model

The modal parameter i.e. frequency, of a thin-walled simply supported curved box-girder model has been found experimentally for a simply supported thin-walled curved box girder model made of Perspex sheets and compared with the finite element results. The model in question has a span of 1.52 metres and a curvature radius of 30.48 metres. The cross-section dimensions are shown in Figure 2. Figure 3 illustrates the tensile strength test specimen that is made of Perspex sheet, whereas Figure 4 demonstrates the Perspex sheet specimen's tensile stress-strain curve. The Young's modulus of Elasticity, Poisson's ratio and Shear modulus of the Perspex box-girder are 2.91 e+9 N/m^2, 0.4 and 1.04e+9 N/m^2 respectively. The complete material properties of the model are listed in Table 1.
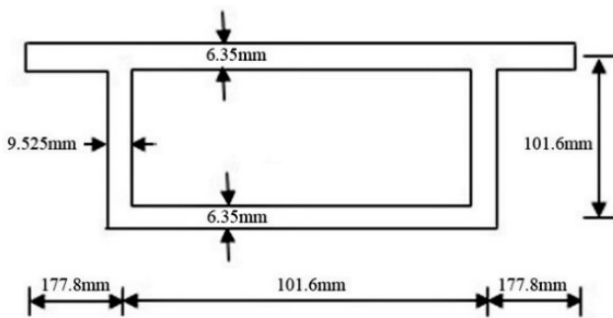
Fig. 2. Cross-section
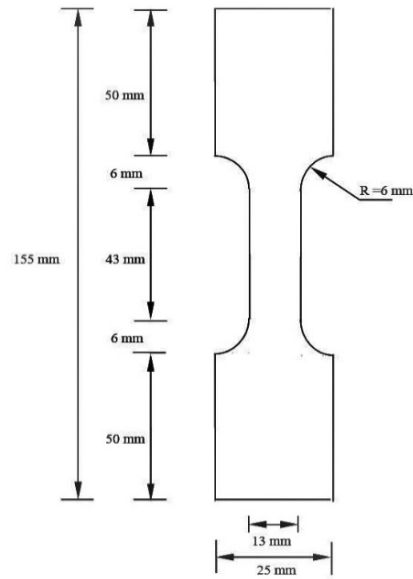
Fig. 3. Tensile strength test specimen made of Perspex sheet
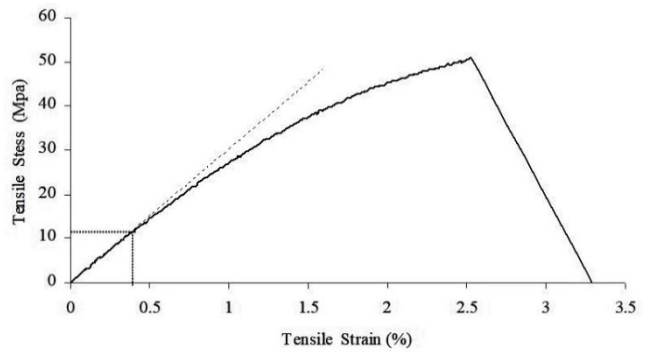
Fig. 4. The Perspex sheet specimen's tensile stress-strain curve

Table 1.
Different material properties

Sectional Property	Value
E	2.91 e+9 N/m^2
ν	0.40
G	1.04e+9N/m^2
I_z	1.11e-5 m^4
J_T	1.89e-5 m^4
J_I	1.43e-8 m^6
J_{II}	1.95e-8 m^6
J_d	6.45e-4 m^2
μ_t	0.365
A	6.0e-3 m^2

The bridge model was exposed to an impact load on its top surface at a specific location by striking the top of the bridge deck with a 150-gram impact hammer. The experimental setup for free vibration study of a curved box girder bridge model is shown in Figure 5, whereas Figure 6 illustrates the entire prototype model.
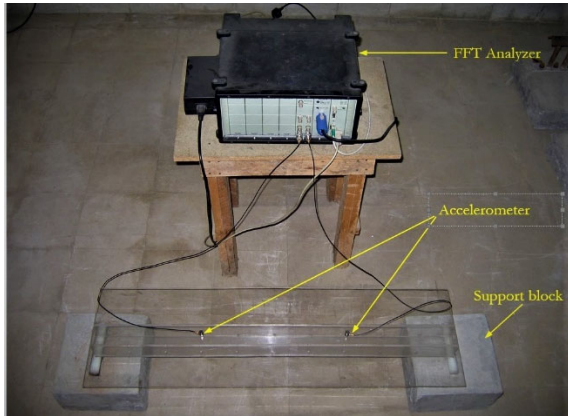
Fig. 5. Experimental setup for free vibration study of a curved box girder bridge model
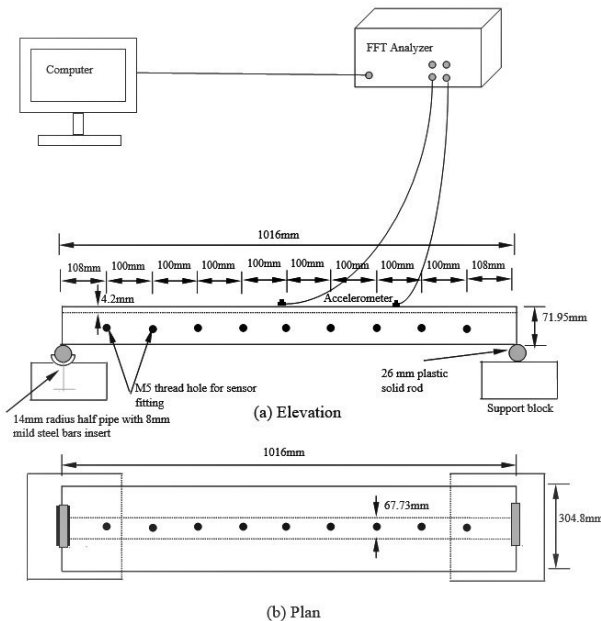
Fig. 6. Representation of the experimental setup for a thin-walled curved box girder model made of Perspex sheets

The accelerometers were connected to input channels in the front end of Fast Fourier Transform analyser. The complete details of accelerometers used for the experiment are given in Table 2. The acquisition front end with AC/DC power supply, 100 kHz input modules, generator modules, signal analyser input modules, and output modules make up the FFT analyser. All digital data communication between the Digital Signal Processing unit (s) and modules in the acquisition front end is handled by the signal analyser interface module. The dynamic range of all input modules is greater than 80 dB. The FFT output channels are connected to a PC loaded with PULSE software, which allows the response signals to be processed.

Table 2.
Details of accelerometers used for the experiment

Property	Type 4371	Type 4381	Type 4396
Type	Charge	Charge	Deltatrone
Frequency range (Hz)	0.2-9100	0.2-3500	1-25000
Sensitivity (pC/ms^{-2})	$1 \pm 2\%$	$10 \pm 2\%$	$10 \pm 2\%$ (mV/ms^{-2})
Weight (grams)	11	43	18.2

Modal data extraction

The damping ratios and modal amplitudes involved with each resonant peak of the measured frequency response function are assessed after the frequency response of a test structure is obtained. The test specimen's frequencies, damping ratios, and mode shape are shown in the following paragraphs.

Natural frequencies and damping ratio

The natural frequencies were determined by looking at the frequencies where the frequency response function's peaks are prominent. The modal damping ratio, ζ_i is considered to be the damping ratio associated with each peak of the frequency response function. For the assessment of the damping ratio, the Half Power Band Width Method was used. The magnitude plot of the frequency response functions (compliance) is used to calculate the modal damping ratios, as seen in Figure 7. Further, the plot of frequency response function for the curved bridge model is shown in Figure 8.

The peak$|H(\omega)|$at resonance is well characterized in systems with low damping. The frequencies corresponding to the two points (a, b) on the magnitude plot are related to the modal damping ratio, where

$$|H(\omega_a)| = |H(\omega_b)| = \frac{|H(\omega_d)|}{\sqrt{2}} \qquad \text{Eq. (23)}$$

The bandwidth $\omega_b - \omega_a$ equals $2\zeta\omega_d$, where

$$\zeta = \frac{\omega_b - \omega_a}{2\omega_d} \qquad \text{Eq. (24)}$$

ω_d, in the above equation corresponds to damped natural frequency at resonance.
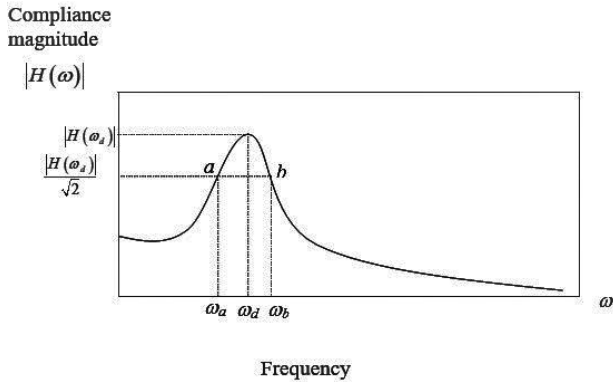
Fig. 7. Magnitude of FRF for estimating modal damping ratio by using Half Power Band Width Method
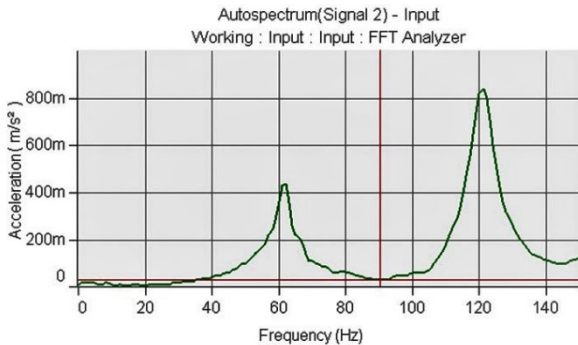

Fig. 8. Plot of the frequency response function for the model of a simply supported curved box girder bridge

Mode shape calculation

Assessing the mode shapes from experimentally determined transfer functions is a little more difficult and requires measuring multiple transfer functions. The Frequency Response Functions (FRF) and subsequent phase angle plot at various sensors location were used to calculate mode shapes. The data from nine sensor locations was used in this analysis. The mode shape was extracted from observed data using Quadratic Peak Picking Method and compared to theoretical results. The basic concept was to create a relationship between the receptance matrix and the system's mode shapes, which could then be used in testing to determine the test specimen mode shapes.

Discussion of Experiment Results

The first two frequencies for the simply supported curved box girder model were experimentally investigated by collecting responses through accelerometers positioned on the curved box girder model along the deck's centre line. Accelerometers were also placed on the box girder's web to detect the lateral mode. The Bruel & Kjaer FFT analyser with in-built PULSE software was used to process the experimental data.

The frequency response for the simply supported curved box girder model during an impact excitation is reliably recorded for the first two modes and hence the results for the first two modes have been presented. The vertical and lateral bending of the bridge specimen refer to these two modes.

Figure 8 illustrates an experimentally obtained Frequency Response Function (FRF). The natural frequencies of the bridge being measured correspond to the FRF's peaks. Table 3 indicates the disparities between theoretical and experimental findings for the first two frequencies along with the experimentally measured damping ratios obtained from the FRF plot using the Quadratic Peak Picking process. Figures 9 and 10 reflect the mode shapes that were observed both theoretically and experimentally. The agreement reached has been deemed acceptable.

Table 3.
Discrepancies in theoretical and experimental findings

Mode sequence	Frequency, Hz		% Difference	Damping Ratio (ζ)
	Theoretical (FEM)	Experimental (FFT)		
First mode (flexural)	59.17	61.50	3.93	0.04509
Second mode (lateral)	116.20	121.00	3.96	0.03361
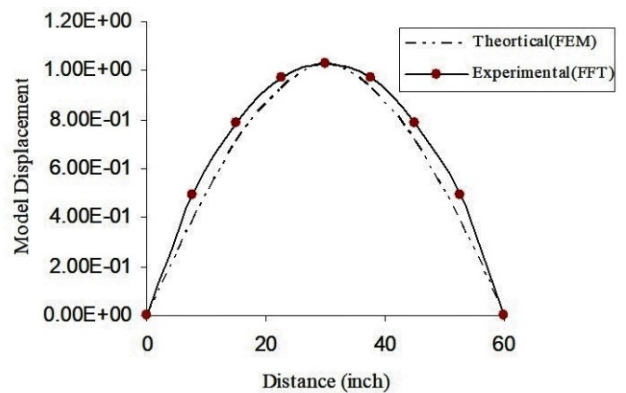
Fig. 9. First mode shape
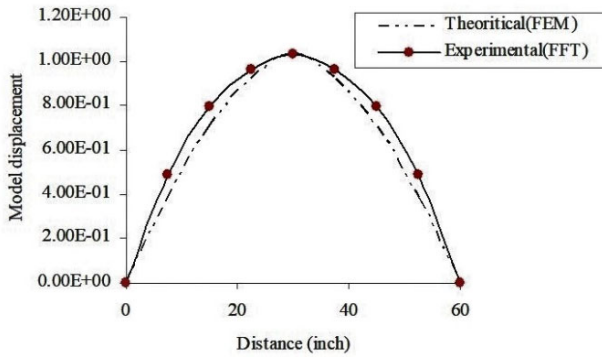
Fig. 10. Second mode shape

5.2. Analytical validation through simply supported concrete box-girder

This numerical example presented by [2] considers a concrete box-girder spanning 30 meters, where the ends are simply supported and braced by diaphragms. The Young's modulus of Elasticity, Poisson's ratio and Shear modulus of the box-girder are 3.45 e+10 N/m², 0.15 and 1.5e+10 N/m² respectively. The various material properties are listed in Table 4. Four degrees of freedom are restricted at hinged support i.e. $u = v = w = \theta_x = 0$, whereas only three are restricted at roller support i.e. $u = v = w = 0$. The cross section has a depth of 1.5 m, a width of 8 m, a web thickness of 0.3 m, an upper flange thickness of 0.25 m and a lower flange thickness of 0.22 m. The complete cross-section details is depicted in Figure 11. The beam is examined with 30 thin-walled box-girder elements. Table 4 depicts the mode

shape diagrams for the first 10 modes, along with the cyclic frequency values. Various modes may be associated with a specific frequency, but the dominant one is more significant, as can be seen in figures of Table 5. The cyclic frequency values continue to increase with each mode and the results are in close resemblance to the research conducted by [8].
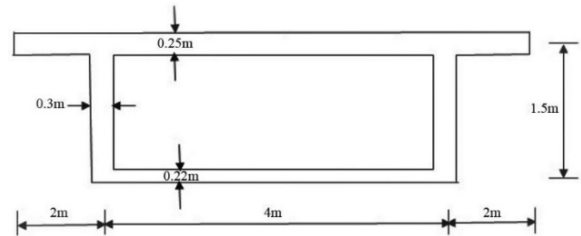
Fig. 11. Straight beam model with dimensions

Table 4.
Different material properties

Sectional Property	Value
E	3.45 e+10 N/m²
ν	0.15
G	1.5e+10N/m²
I_z	1.606 m⁴
J_T	3.259 m⁴
J_I	0.793 m⁶
J_{II}	1.013 m⁶
J_d	0.005 m²
μ_t	0.365
A	3.705 m²

Table 5.
Mode shapes for box-girder bridge

Mode	DOF	Cyclic frequency, Hz	Mode Shape
1	v (1ˢᵗVertical Mode)	4.33	
2	w (1ˢᵗ Lateral Mode)	12.69	

Mode	DOF	Cyclic frequency, Hz	Mode Shape
3	v (2nd Vertical Mode)	16.80	
4	γ_d (1st Distortional Mode)	23.87	
5	γ_d (2nd Distortional Mode)	26.95	
6	u (1st Axial Mode)	31.57	
7	v (3rd Vertical Mode)	36.39	
8	γ_d (3rd Distortional Mode)	37.56	
9	θ_x (1st Torsional Mode)	38.99	

Mode	DOF	Cyclic frequency, Hz	Mode Shape
10	w (2nd Lateral Mode)	44.58	

Table 6.
Cyclic frequency variation with elements

Mode \ Element	8 Element	30 Element	100 Element	300 Element	500 Element
Mode 1 (v 1st Vertical Mode)	4.22	4.21	4.21	4.21	4.30
Mode 2 (w 1st Lateral Mode)	11.68	11.68	11.68	11.68	11.68
Mode 3 (v 2nd Vertical Mode)	16.37	16.26	16.26	16.26	16.24
Mode 4 (γ_d 1st Distortional Mode)	23.85	23.85	23.85	23.85	23.85
Mode 5 (γ_d 2nd Distortional Mode)	26.66	26.66	26.66	26.66	26.67
Mode 6 (u 1st Axial Mode)	31.08	31.07	31.07	31.07	31.08
Mode 7 (v 3rd Vertical Mode)	33.82	33.48	33.48	33.48	33.47
Mode 8 (γ_d 3rd Distortional Mode)	36.51	36.51	36.51	36.51	36.55
Mode 9 (θ_x 1st Torsional mode)	40.25	40.09	40.09	40.09	40.09
Mode 10 (w 2nd Lateral Mode)	44.85	44.80	44.80	44.80	44.80
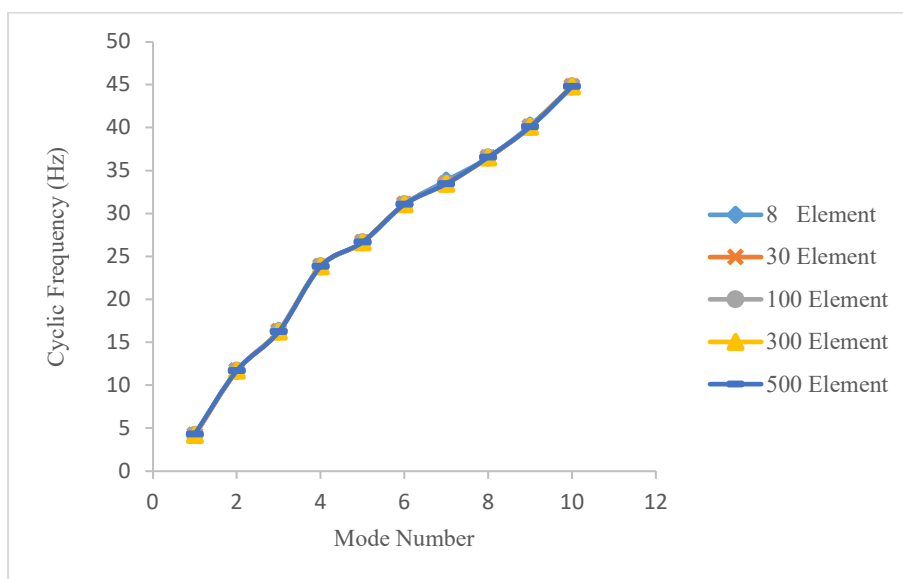
Fig. 12. Cyclic frequency variation with elements

6. Parametric study on concrete box-girder model

A parametric study is conducted on the above concrete box-girder model to identify various factors affecting the cyclic frequency of the box-girder bridge. Following are the key parameters considered in this study:

1. Element discretization,
2. Radius of curvature,
3. Span length,
4. Boundary condition,
5. Diaphragm arrangement,
6. Cross-section of box-girder.

6.1. Effect of element discretization

The variation of first ten cyclic frequency for the concrete bridge of radius 40 meters and span 30 meters is demonstrated in Table 6. The analysis has been done on the basis of variations in the number of elements in which the ends are simply supported and braced with rigid diaphragms. Two significant trends can be drawn from the results. First, the cyclic frequency values tend to escalate with each mode, and second, the discretization of the elements does not have a major impact on cyclic frequency. The values of all modes remain more or less the same for all the elements. Figure 12 illustrates the variation of cyclic frequency with different number of elements.

6.2. Effect of radius of curvature

The effects of radius of curvature ranging from 40 meters to 360 meters on the first ten natural frequencies of simply-supported concrete box-girder bridge with a 30 meter span and end diaphragm are shown in Figure 13. It is interesting to note that the fundamental frequencies tend to increase with an increase in curvature, except for torsional and 2nd Lateral Mode, as shown in Table 7. It is worth mentioning that 1st Lateral mode, 3rd Vertical mode and 3rd Distortional mode appear to increase more than other modes. A maximum increase of 7.19% is observed in 3rd Vertical mode as the radius varies from 40 meters to 360 meters. Hence, it can be said that the fundamental frequencies begin to increase as the curvature increases. However, curvature radius do not have a noticeable impact on the frequency of most practical box girder bridges as discussed by (Huang), (2001) in [48].

6.3. Effect of span

It has long been recognized that span length has a significant effect on the free vibration characteristics of curved bridges [45]. Figure 14 highlights the influence of the span length on the first ten natural frequencies of simply-supported concrete box-girder bridge spanning 30, 45, 60 and 75 meters with radius of curvature 40 meters and having end diaphragms. Natural frequencies decrease with
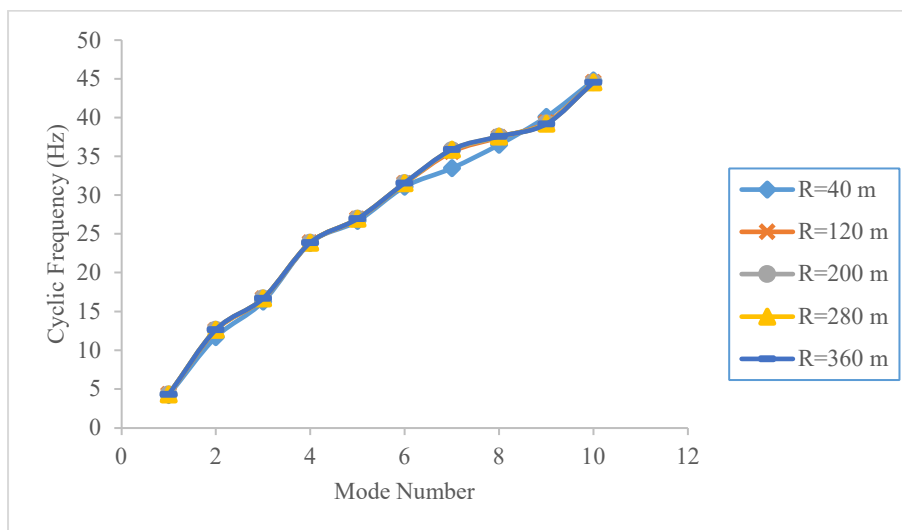

Fig. 13. Cyclic Frequency variation with Radius of curvature

Table 7.
Cyclic Frequency variation with radius of curvature

Mode \ Radius	R=40 m	R=120 m	R=200 m	R=280 m	R=360 m
Mode 1 (v 1st Vertical Mode)	4.21	4.29	4.30	4.30	4.30
Mode 2 (w 1st Lateral Mode)	11.68	12.56	12.64	12.66	12.66
Mode 3 (v 2nd Vertical Mode)	16.26	16.66	16.69	16.70	16.70
Mode 4 (γ_d 1st Distortional Mode)	23.85	23.86	23.86	23.86	23.86
Mode 5 (γ_d 2nd Distortional Mode)	26.66	26.93	26.95	26.95	26.96
Mode 6 (u 1st Axial Mode)	31.07	31.52	31.55	31.56	31.57
Mode 7 (v 3rd Vertical Mode)	33.48	35.58	35.80	35.87	35.89
Mode 8 (γ_d 3rd Distortional Mode)	36.51	37.46	37.54	37.56	37.57
Mode 9 (θ_x 1st Torsional mode)	40.09	39.36	39.24	39.21	39.19
Mode 10 (w 2nd Lateral Mode)	44.80	44.56	44.54	44.53	44.53
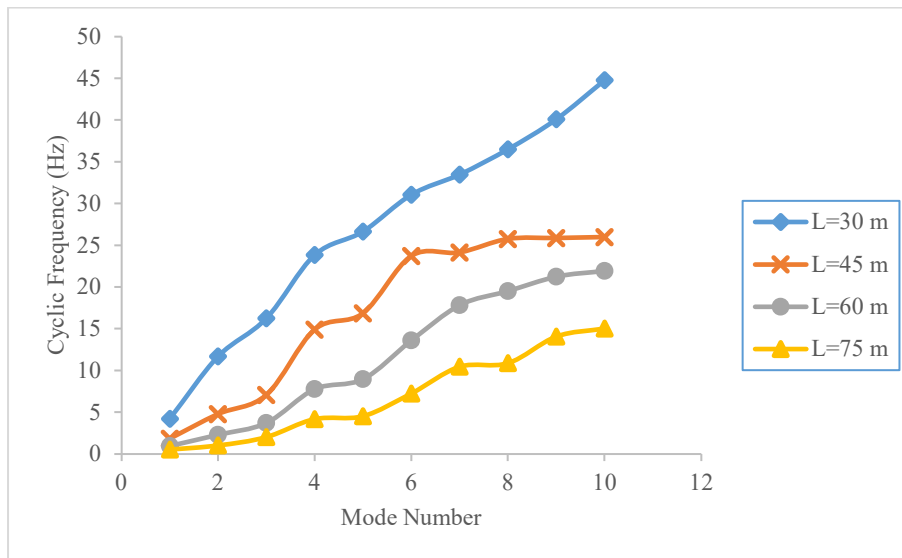
Fig. 14. Cyclic frequency variation with span length

increasing bridge span length for all lower as well as higher degree of freedom modes, as can be seen in Table 8. Compared to other modes, the first three modes decrease quite dramatically and a maximum decrease of 91.22% is observed in 1st Lateral Mode as the span changes from 30 meters to 75 meters. It is worthwhile noticing that all the modes have a greater tendency to change as the span changes. In the case of radius, this pattern was different, where all modes were less inclined to vary. Therefore, it can be inferred that span length has a noticeable impact on the natural frequencies of curved box-girder bridge and needs to be included in the parametric analysis.

6.4. Effect of boundary conditions

The influence of boundary conditions on the free vibration response of the concrete box girder bridge has been investigated in this section. The various boundary conditions for a fixed support are: $u = v = w = 0$, $\theta_x = \theta_y = \theta_z = 0$, $\theta_x' = \gamma_d = \gamma_a' = 0$, for a pinned support with a Rigid Diaphragm are: $u = v = w = 0$, $\theta_x = \gamma_d = 0$, for a linear roller with a Rigid diaphragm are: $v = w = 0$, $\theta_x = \gamma_d = 0$. The first ten frequencies for four different boundary condition cases: Cantilever, Simply Supported, Fixed, and

Table 8.
Cyclic frequency variation with span length

Mode \ Span	L=30 m	L=45 m	L=60 m	L=75 m
Mode 1 (v 1st Vertical Mode)	4.21	1.82	0.96	0.54
Mode 2 (w 1st Lateral Mode)	11.68	4.80	2.28	1.02
Mode 3 (v 2nd Vertical Mode)	16.26	7.08	3.73	2.02
Mode 4 ($\gamma_d 1^{st}$ Distortional Mode)	23.85	14.91	7.76	4.19
Mode 5 ($\gamma_d 2^{nd}$ Distortional Mode)	26.66	16.86	8.96	4.53
Mode 6 (u 1st Axial Mode)	31.07	23.73	13.60	7.25
Mode 7 (v 3rd Vertical Mode)	33.48	24.16	17.83	10.45
Mode 8 ($\gamma_d 3^{rd}$ Distortional Mode)	36.51	25.77	19.50	10.87
Mode 9 ($\theta_x 1^{st}$ Torsional mode)	40.09	25.89	21.23	14.05
Mode 10 (w 2nd Lateral Mode)	44.80	26.01	21.94	15.03

Table 9.
Cyclic Frequency variation with Support Condition

Mode \ Support	Cantilever	Simply Supported	Fixed	Continuous
Mode 1 (v 1st Vertical Mode)	1.49	4.21	8.92	34.96
Mode 2 (w 1st Lateral Mode)	4.47	11.68	23.81	36.50
Mode 3 (v 2nd Vertical Mode)	8.31	16.26	24.75	42.47
Mode 4 ($\gamma_d 1^{st}$ Distortional Mode)	20.45	23.85	26.42	42.55
Mode 5 ($\gamma_d 2^{nd}$ Distortional Mode)	21.80	26.66	30.80	57.43
Mode 6 (u 1st Axial Mode)	24.15	31.078	42.76	58.32
Mode 7 (v 3rd Vertical Mode)	24.88	33.48	44.50	59.34
Mode 8 ($\gamma_d 3^{rd}$ Distortional Mode)	28.46	36.51	44.84	80.88
Mode 9 ($\theta_x 1^{st}$ Torsional mode)	34.33	40.09	50.94	90.95
Mode 10 (w 2nd Lateral Mode)	40.42	44.80	65.33	103.87

Continuous of the analytical bridge are listed in Table 9. The radius and length of the bridge are 40 meters and 30 meters respectively. Figure 15 demonstrates the variation of cyclic frequency with different support conditions. It is evident that the fundamental frequency is increasing in all degree of freedom modes for all support conditions. Cyclic frequencies are the least for cantilever case and maximum for continuous boundary condition for all the modes. The cyclic frequency of continuous boundary condition goes as high as 103.87 Hz for the tenth mode, which is the maximum for all the cases considered in this parametric study.

6.5. Effect of diaphragm arrangement

Diaphragms, also known as cross-braces, serve as primary load-bearing components in bridges and must therefore be included in the parametric analysis. Diaphragms can be provided in the form of steel plates and are normally designed as deep beams, the depth of which exceeds the width by two times. The diaphragm study has been conducted by putting $\gamma_d = 0$ in the analysis. In the case of no diaphragm, this condition has not been taken into account as can be seen by Huang and Wang, 1998 in [49]. The first ten frequencies are examined for three separate cases of Diaphragm: End Diaphragm, Intermediate Diaphragm and No Diaphragm. The radius and span of the simply supported concrete box-girder bridge are taken as 40 meters and 30 meters respectively. No diaphragm is considered in case-I and in case-II, the diaphragm is assumed to be rigid at the end supports. In Case-III, the intermediate Diaphragm with a spacing of 1/8 of the bridge span and with the same rigidity as the end Diaphragm is included. Figure 16 illustrates the cyclic frequency
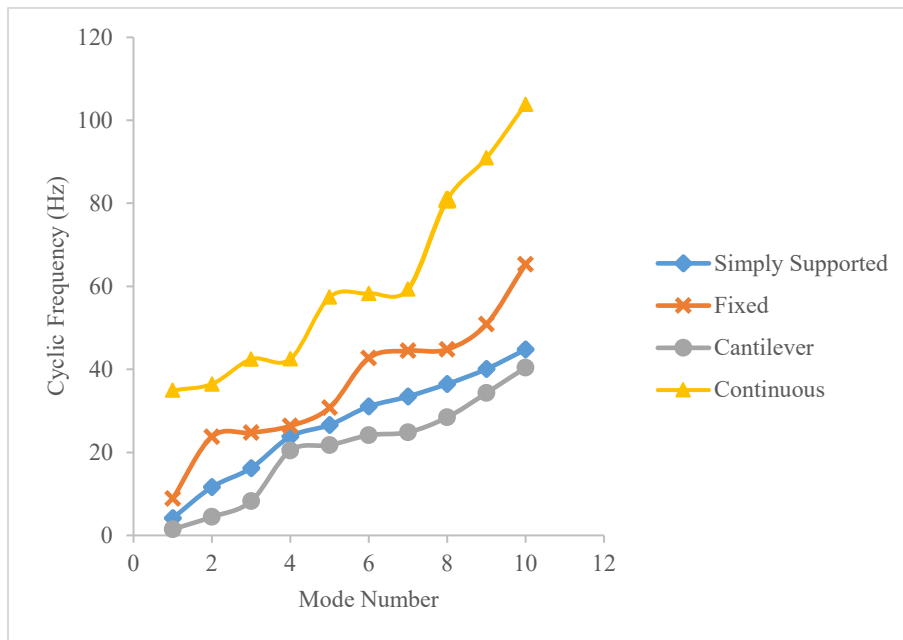
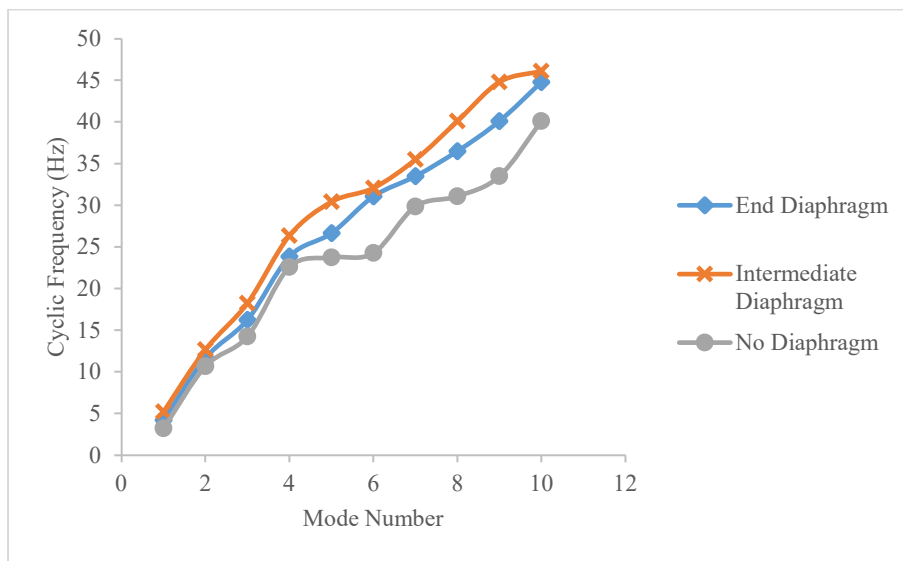Fig. 15. Cyclic Frequency variation with Support Condition

Fig. 16. Cyclic Frequency variation with Diaphragm

variation with various diaphragm configurations. An investigation into Table 10 goes to show that in all three cases, the cyclic frequency values increase for all modes. Also, Case-III recorded the maximum cyclic frequency values, while the Case-I values were the least for all modes.

6.6. Effect of cross-section

Four different cross-sections have been taken to assess their impact on free vibration characteristics of simply supported concrete box-girder bridge of 30 meters length and 40 meters radius with end diaphragms.

Table 10.
Cyclic Frequency variation with Diaphragm

Mode	No Diaphragm	End Diaphragm	Intermediate Diaphragm
Mode 1 (v 1st Vertical Mode)	3.21	4.21	5.21
Mode 2 (w 1st Lateral Mode)	10.68	11.68	12.68
Mode 3 (v 2nd Vertical Mode)	14.26	16.26	18.26
Mode 4 (γ_d 1st Distortional Mode)	22.59	23.85	26.36
Mode 5 (γ_d 2nd Distortional Mode)	23.74	26.66	30.42
Mode 6 (u 1st Axial Mode)	24.27	31.07	32.07
Mode 7 (v 3rd Vertical Mode)	29.86	33.48	35.48
Mode 8 (γ_d 3rd Distortional Mode)	31.07	36.51	40.09
Mode 9 (θ_x 1st Torsional mode)	33.48	40.09	44.80
Mode 10 (w 2nd Lateral Mode)	40.09	44.80	46.09

Table 11.
Cyclic Frequency variation with Cross-section

Mode	Single cell rectangular	Single cell tapered	Double cell rectangular	Double spined tapered
Mode 1 (v 1st Vertical Mode)	4.21	3.09	2.25	0.95
Mode 2 (w 1st Lateral Mode)	11.68	7.38	3.50	1.76
Mode 3 (v 2nd Vertical Mode)	16.26	11.93	5.20	3.75
Mode 4 (γ_d 1st Distortional Mode)	23.85	23.02	8.04	6.93
Mode 5 (γ_d 2nd Distortional Mode)	26.66	24.63	8.30	7.51
Mode 6 (u 1st Axial Mode)	31.07	29.88	10.22	7.54
Mode 7 (v 3rd Vertical Mode)	33.48	30.51	11.31	7.56
Mode 8 (γ_d 3rd Distortional Mode)	36.51	42.50	11.73	7.62
Mode 9 (θ_x 1st Torsional mode)	40.09	45.95	15.51	7.62
Mode 10 (w 2nd Lateral Mode)	44.80	45.96	15.52	7.67

The cross-sections taken are single cell rectangular, single cell tapered, double cell rectangular and double spined tapered respectively as shown in Table 11. Figure 17 clearly shows that cyclic frequency values for the double cell box-section are substantially reduced relative to single cell box sections. This is due to the fact that as cell number increases, stiffness decreases, resulting in lower cyclic frequencies. It can also be seen that the cyclic frequencies are more for single cell rectangular as compared to single cell tapered case for all the modes. The same pattern is observed in double cell rectangular and double spined tapered case, where the cyclic frequency values of double cell rectangular cross-section exceeds the double spined tapered case for all

the modes. In this parametric study, the frequency value of 0.95 Hz is recorded as the lowest value for the first mode of double spined tapered case.

7. Conclusions

The bridge curved in plan has been modelled using a computationally less expensive and practical three noded thin-walled box beam element. The pertinence of such an element for dynamic analysis has been confirmed both experimentally and analytically by testing the modal parameters of the curved box girder model. In addition,
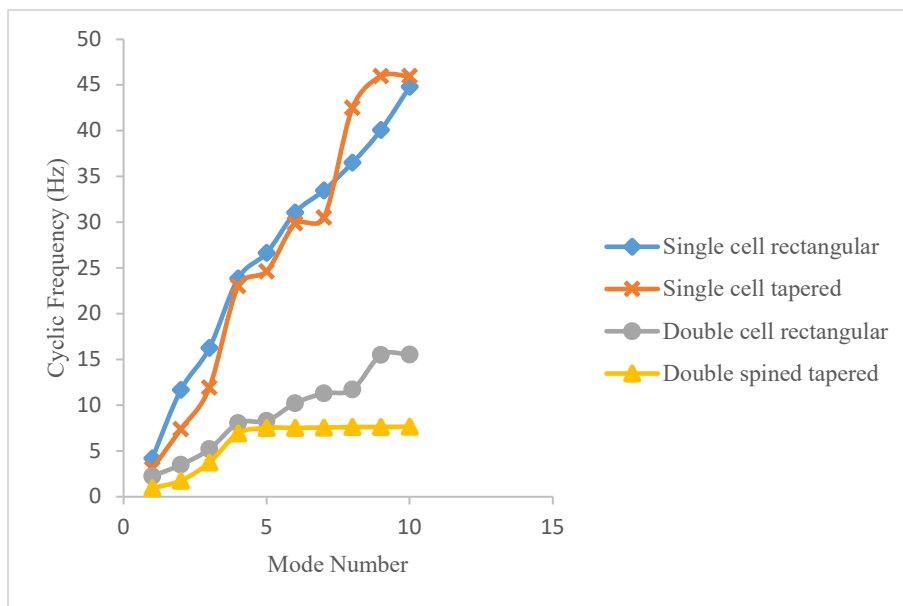
Fig. 17. Cyclic Frequency variation with Cross-section

a parametric study of the concrete box-girder model was performed in order to identify various factors influencing its cyclic frequency.

The conclusions drawn from the study are as follows:

1. The paper evaluates six different parameters of a concrete box-girder bridge that affects its free vibration response based on three noded, one-dimensional, thin-walled box beam element developed by Zhang and Lyons in [46].

2. The results found experimentally as well as analytically are in excellent agreement with the findings of previous studies, which illustrates the authenticity of the given numerical formulation.

3. The research carried out is for a curved concrete, thin-walled box-girder bridge, which can be extended to a steel box-girder bridge.

4. It is observed that the fundamental frequencies increase with an increase in radius and decrease with an increase in span length of the bridge barring certain exceptions.

5. The cantilever boundary condition case recorded the lowest values of cyclic frequencies, while the maximum values were for the continuous boundary condition case for all modes.

6. The study showed that the cyclic frequencies increase with the introduction of diaphragms and the maximum values were obtained when intermediate diaphragms were placed.

7. Double cell box-sections can be used instead of single cell box-sections if different modes are to be stimulated at lower frequencies.

References

[1] C.P. Heins Jr., J.C. Oleinik, Curved box beam bridge analysis, Computers & Structures 6/2 (1976) 65-73. DOI: https://doi.org/10.1016/0045-7949(76)90054-7

[2] B. Kermani, P. Waldron, Analysis of continuous box girder bridges including the effects of distortion, Computers & Structures 47/3 (1993) 427-440. DOI: https://doi.org/10.1016/0045-7949(93)90238-9

[3] M. Mukhopadhyay, A.H. Sheikh, Large amplitude vibration of horizontally curved beams: a finite element approach, Journal of Sound and Vibration 180/2 (1995) 239-251.
DOI: https://doi.org/10.1006/jsvi.1995.0077

[4] D.J. Ewins, Modal Testing: Theory, Practice, and Application, Research Studies Press, Hertfordshire, England, 2000.

[5] M.I. Friswell, J.E. Mottershead, Finite Element Model Updating in Structural Dynamics, Kluwer Academic Publishers, Dordrecht, Boston and London, 1995.

[6] W.X. Ren, G. De Roeck, Structural damage identification using modal data. I: Simulation

verification, Journal of Structural Engineering 128/1 (2002) 87-95.
DOI: https://doi.org/10.1061/(ASCE)0733-9445(2002)128:1(87)

[7] W.X. Ren, G.E. Blandford, I.E. Harik, Roebling suspension bridge. I: Finite-element model and free vibration response, Journal of Bridge Engineering 9/2 (2004) 110-118.
DOI: https://doi.org/10.1061/(ASCE)1084-0702(2004)9:2(110)

[8] K. Nallasivam, Response of horizontally curved thin-walled box-girder bridge to vehicular loads, PhD Thesis, Indian Institute of Technology Guwahati, India, 2006. Available from:
http://gyan.iitg.ernet.in/handle/123456789/106

[9] V.Z. Vlasov, Beams TW Chapter V, National Science Foundation, Washington, DC, 1961.

[10] B.I. Maisel, Analysis of concrete box beams using small computer capacity, Canadian Journal of Civil Engineering 12/2 (1985) 265-278.
DOI: https://doi.org/10.1139/l85-028

[11] L.F. Boswell, Q. Li, Consideration of the relationships between torsion, distortion and warping of thin-walled beams, Thin-walled Structures 21/2 (1995) 147-161.
DOI: https://doi.org/10.1016/0263-8231(94)00030-4

[12] J. Jönsson, Distortional warping functions and shear distributions in thin-walled beams, Thin-Walled Structures 33/4 (1999) 245-268.
DOI: https://doi.org/10.1016/S0263-8231(98)00048-2

[13] H. Zhang, R. DesRoches, Z. Yang, S. Liu, Experimental and analytical studies on a streamlined steel box girder, Journal of Constructional Steel Research 66/7 (2010) 906-914. DOI: https://doi.org/10.1016/j.jcsr.2010.02.001

[14] M.R. Awall, T. Hayashikawa, T. Matsumoto, X. He, Effects of bottom bracings on torsional dynamic characteristics of horizontally curved twin I-girder bridges with different curvatures, Earthquake Engineering and Engineering Vibration 11/2 (2012) 149-162. DOI: https://doi.org/10.1007/s11803-012-0106-4

[15] G.C. Ezeokpube, S.B. Singh, N.N. Osadebe, Numerical and Experimental Modeling of the Static Response of Simply Supported Thin-Walled Box Girder Bridges, Nigerian Journal of Technology 34/4 (2015) 685-698.
DOI: https://doi.org/10.4314/njt.v34i4.4

[16] K. Kashefi, A.H. Sheikh, M.C. Griffith, M.M. Ali, K. Tateishi, Static and vibration characteristics of thin-walled box beams: an experimental investigation, Advances in Structural Engineering 20/10 (2017) 1540-1559.
DOI: https://doi.org/10.1177/1369433216687565

[17] I.N. Tsiptsis, E.J. Sapountzakis, Isogeometric analysis for the dynamic problem of curved structures including warping effects, Mechanics Based Design of Structures and Machines 46/1 (2018) 66-84.
DOI: https://doi.org/10.1080/15397734.2016.1275974

[18] I.N. Tsiptsis, E.J. Sapountzakis, Generalized warping and distortional analysis of curved beams with isogeometric methods, Computers & Structures 191 (2017) 33-50.
DOI: https://doi.org/10.1016/j.compstruc.2017.06.007

[19] E.J. Sapountzakis, I.N. Tsiptsis, B-splines in the Analog Equation Method for the generalized beam analysis including warping effects, Computers & Structures 180 (2017) 60-73.
DOI: https://doi.org/10.1016/j.compstruc.2016.03.007

[20] I.N. Tsiptsis, E.J. Sapountzakis, Higher order beam theories and isogeometric methods in the analysis of curved bridges-assessment of diaphragms' guidelines, International Journal of Bridge Engineering 5/3 (2017) 133-182. Available from:
https://www.ijbe.net/issues/volumes/itemlist/category/42-issue-3-sep-dec-2017

[21] M.S. Cheung, Y.K. Cheung, Analysis of curved box girder bridges by finite strip method, Publications IABSE 31/I (1971) 1-19. Available from:
http://hdl.handle.net/1783.1/40444

[22] M.A. Abdullah, A.A. Abdul-Razzak, Finite strip analysis of prestressed box-girders, Computers & Structures 36/5 (1990) 817-822.
DOI: https://doi.org/10.1016/0045-7949(90)90152-R

[23] A. Fam, C. Turkstra, A finite element scheme for box bridge analysis, Computers & Structures 5/2 (1975) 179-186. DOI: https://doi.org/10.1016/0045-7949(75)90008-5

[24] G.A. Gunnlaugsson, P.T. Pedersen, A finite element formulation for beams with thin walled cross-sections, Computers & Structures 15/6 (1982) 691-699. DOI: https://doi.org/10.1016/S0045-7949(82)80011-4

[25] L.F. Boswell, S.H. Zhang, The effect of distortion in thin-walled box-spine beams, International Journal of Solids and Structures 20/9-10 (1984) 845-862. DOI: https://doi.org/10.1016/0020-7683(84)90054-4

[26] Y.T. Hsu, C.C. Fu, D.R. Schelling, An improved horizontally-curved beam element, Computers & Structures 34/2 (1990) 313-318.

DOI: https://doi.org/10.1016/0045-7949(90)90375-C

[27] A.G. Razaqpur, H.G. Li, Refined analysis of curved thin-walled multicell box girders, Computers & Structures 53/1 (1994) 131-142.
DOI: https://doi.org/10.1016/0045-7949(94)90136-8

[28] W. Yaping, L. Yuanming, Z. Yuanin, P. Weidong, A curved box beam element considering shear lag effect and its static and dynamic applications, Journal of Sound and Vibration 253/5 (2002) 1131-1139. Available from: http://pascal-francis.inist.fr/vibad/index.php?action=getRecordDetail&idt=13760506

[29] Z. Begum, Analysis and behaviour investigations of box girder bridges, PhD Thesis, University of Maryland, College Park, USA, 2010.
Available from: http://hdl.handle.net/1903/10500

[30] I.N. Tsiptsis, O.E. Sapountzaki, Analysis of composite bridges with intermediate diaphragms & assessment of design guidelines, Computers & Structures 234 (2020) 106252.
DOI: https://doi.org/10.1016/j.compstruc.2020.106252

[31] Z. Zhu, L. Zhang, D. Zheng, G. Cao, Free vibration of horizontally curved thin-walled beams with rectangular hollow sections considering two compatible displacement fields, Mechanics Based Design of Structures and Machines 44/4 (2016) 354-371. DOI: https://doi.org/10.1080/15397734.2015.1075410

[32] T. Gupta, M. Kumar, Flexural response of skew-curved concrete box-girder bridges, Engineering Structures 163 (2018) 358-372.
DOI: https://doi.org/10.1016/j.engstruct.2018.02.063

[33] Computers & Structures, INC, Structural and Earthquake Engineering Software, Introduction to CSI Bridge, 2017, U.S.A.

[34] B.A. Hamza, A.R. Radhi, Q. Al-Madhlom, Effect of (B/D) ratio on ultimate load capacity for horizontally curved box steel beam under out of plane concentrated load, Engineering Science and Technology: an International Journal 22/2 (2019) 533-537. DOI: https://doi.org/10.1016/j.jestch.2018.09.007

[35] A.K. Noor, J.M. Peters, B.J. Min, Mixed finite element models for free vibrations of thin-walled beams, Finite Elements in Analysis and Design 5/4 (1989) 291-305.
DOI: https://doi.org/10.1016/0168-874X(89)90009-7

[36] M.A. Panicker, A. Mathai, Free vibration analysis on FRP bridges, American Journal of Engineering Research 4 (2013) 47-50.

[37] K.Y. Yoon, Y.J. Kang, Y.J. Choi, N.H. Park, Free vibration analysis of horizontally curved steel I-girder bridges, Thin-Walled Structures 43/4 (2005) 679-699.
DOI: https://doi.org/10.1016/j.tws.2004.07.020

[38] J.M. Snyder, J.F. Wilson, Free vibrations of continuous horizontally curved beams, Journal of Sound and Vibration 157/2 (1992) 345-355. DOI: https://doi.org/10.1016/0022-460X(92)90686-R

[39] M.M. Tabba, C.J. Turkstra, Free vibrations of curved box girders, Journal of Sound and Vibration 54/4 (1977) 501-514. DOI: https://doi.org/10.1016/0022-460X(77)90608-3

[40] T.J. Memory, D.P. Thambiratnam, G.H. Brameld, Free vibration analysis of bridges, Engineering Structures 17/10 (1995) 705-713.
DOI: https://doi.org/10.1016/0141-0296(95)00037-8

[41] C.H. Kou, S.E. Benzley, J.Y. Huang, D.A. Firmage, Free vibration analysis of curved thin-walled girder bridges, Journal of Structural Engineering 118/10 (1992) 2890-2910.
DOI: https://doi.org/10.1061/(ASCE)0733-9445(1992)118:10(2890)

[42] G. Tan, W. Wang, Y. Jiao, Free vibration analysis of a cracked simply supported bridge considering bridge-vehicle interaction, Journal of Vibroengineering 18/6 (2016) 3608-3635.
DOI: https://doi.org/10.21595/jve.2016.16908

[43] M.R. Awall, T. Hayashikawa, T. Humyra, M.B. Zisan, Free vibration characteristics of horizontally curved continuous multi I-girder bridge, Proceedings of the 3rd International Conference on Civil Engineering for Sustainable Development (ICCESD 2016), KUET, Khulna, Bangladesh, 2016, 730-736.

[44] H. Yin, Z. Li, and X. Hao, Research on structural dynamic characteristics of continuous steel box girder-bridge with lager ratio of wide-span, ITM Web of Conferences 17 (2018) 03008.
DOI: https://doi.org/10.1051/itmconf/20181703008

[45] R. Wodzinowski, K. Sennah, H.M. Afefy, Free vibration analysis of horizontally curved composite concrete-steel I-girder bridges, Journal of Constructional Steel Research 140 (2018) 47-61. DOI: https://doi.org/10.1016/j.jcsr.2017.10.011

[46] V. Verma, K. Nallasivam, One-dimensional finite element analysis of thin-walled box-girder bridge, Innovative Infrastructure Solutions 5 (2020) 51. DOI: https://doi.org/10.1007/s41062-020-00287-x

[47] S.H. Zhang, L.P.R. Lyons, A thin-walled box beam finite element for curved bridge analysis, Computers & Structures 18/6 (1984) 1035-1046. DOI: https://doi.org/10.1016/0045-7949(84)90148-2

[48] D. Huang, Dynamic analysis of steel curved box girder bridges, Journal of Bridge Engineering 6 (2001) 506-513. DOI: https://doi.org/10.1061/(ASCE)1084-0702(2001)6:6(506)

[49] D. Huang, T.L. Wang, M. Shahawy, Vibration of horizontally curved box girder bridges due to vehicles, Computers & Structures 68/5 (1998) 513-528. DOI: https://doi.org/10.1016/S0045-7949(98)00065-0